HHS Public Access

Author manuscript

Science. Author manuscript; available in PMC 2024 March 25.

Published in final edited form as:

Science. 2023 July 28; 381(6656): 420–427. doi:10.1126/science.adi1024.

Climbing fiber multi-innervation of mouse Purkinje dendrites with arborization common to human

Silas E. Busch[1], **Christian Hansel**[1,*]

[1]Department of Neurobiology and Neuroscience Institute, University of Chicago, Chicago, IL 60637, USA.

Abstract

Canonically, each Purkinje cell (PC) in the adult cerebellum receives only one climbing fiber (CF) from the inferior olive. Underlying current theories of cerebellar function is the notion that this highly conserved one-to-one relationship renders Purkinje dendrites into a single computational compartment. However, we discovered that multiple primary dendrites are a near-universal morphological feature in humans. Using tract tracing, immunolabeling, and in vitro electrophysiology, we found that in mice ~25% of mature multibranched cells receive more than one CF input. Two-photon calcium imaging in vivo revealed that separate dendrites can exhibit distinct response properties to sensory stimulation, indicating that some multibranched cells integrate functionally independent CF-receptive fields. These findings indicate that PCs are morphologically and functionally more diverse than previously thought.

Editor's summary

Purkinje cells are the primary output neurons of the cerebellum. It is generally thought that one Purkinje cell receives monosynaptic input from one climbing fiber, which forms many excitatory synapses with it. Busch and Hansel found that in contrast to the assumed universal one-to-one relationship, most Purkinje cells in the adult human cerebellum receive multiple climbing fiber inputs. In mice, multibranched Purkinje cells show more than one climbing fiber input. This innervation pattern generates independent computational compartments within single Purkinje cells. These results indicate that there is more anatomical and functional Purkinje cell diversity than traditionally assumed and that there are substantial differences in the prevalence of multibranched cells between mouse and human, where this dendrite type is predominant. —PRS

*Corresponding author. chansel@bsd.uchicago.edu.

Author contributions: S.E.B. and C.H. designed the experiments. S.E.B. performed the investigation, formal analysis, visualization, and wrote the original draft. S.E.B. and C.H. acquired funding and edited the text. C.H. supervised the work.

Competing interests: Authors declare that they have no competing interests.

Data and materials availability: All data are available in the manuscript or the supplementary materials. Data and post-processing analysis code are publicly available in a Dryad archive (62).

SUPPLEMENTARY MATERIALS

science.org/doi/10.1126/science.adi1024

Inputs to the cerebellar cortex are integrated by the dendrites of Purkinje cells (PCs), its sole cortical output neuron. Despite their well-characterized position in what is considered a conserved and stereotypical circuit (1), PCs exhibit diverse dendritic morphology in rodents (2) and it is not known how specific features of dendritic arborization may affect their function.

Human PC morphology remains even more elusive. Studies of human PC morphology, which date back more than 120 years to the iconic illustrations of Golgi and Ramón y Cajal (3, 4), typically investigate small numbers of cells (5-7). Although no quantitative information on frequency and distribution of morphological types is available, it can be observed that human PCs are often “multibranched,” having either numerous trunks emerging from the soma or a proximal bifurcation of a single trunk. These features produce highly segregated dendritic compartments, raising the question of whether this confers functional properties that have gone unreported.

We specifically asked whether the existence of several primary dendrites enables multiple climbing fiber (CF) innervation in the adult cerebellum. During development, the early growth of a primary dendrite provides structural support for the ramification of a “winner” CF amidst competitive elimination of surplus CFs (8-10). Weaker CF inputs fail to translocate to the dendrite, possibly as a result of competitive processes resembling adult bidirectional synaptic plasticity (11-14). In PCs where multiple primary dendrites conceivably offer a means to evade competition from other CFs, is the elimination pressure reduced enough to allow multiple CFs to be maintained? Would multi-innervation provide functionally independent receptive fields to distinct dendritic compartments?

A majority of human, but not murine, PCs have multiple primary dendrites

We used fluorescent calbindin immunolabeling to visualize PCs in postmortem human tissue (Fig. 1A). Based on proximal primary dendrite structure, which articulates the contours of the entire arbor, we define one standard structural category—Normative, in which one primary dendrite may have a distant bifurcation (beyond a two-somatic diameter threshold of 40 μm in mice and 50 to 70 μm in humans)–and two multibranched categories—Split, in which there is one trunk that bifurcates into multiple primary dendrites proximal to the soma (below the somatic diameter threshold) and Poly—, in which multiple trunks emerge directly from the soma (Fig. 1A and fig. S1; see materials and methods). Although these categories translate to mice (Fig. 1D), we found that mice diverged significantly from humans in that they had fewer Split PCs (35.9 versus 44.8%) and far fewer Poly PCs (16.6 versus 51.2%; Fig. 1G and fig. S2A). Instead, in mice Normative PCs constituted the largest PC category (47.5%) in contrast to humans (4.0%).

We manually marked the distribution of dendritic morphologies of collectively ~8000 cells across whole parasagittal reconstructions of brain slices from the mid-hemisphere in humans and mice (Fig. 1, B and E, and fig. S2, B and C). In posterior lobules of humans, there is a higher percentage of Poly PCs (53.8 versus 40.9%) and a lower percentage of Normative PCs (3.5 versus 6.1%) than in anterior lobules (Fig. 1C, fig. S2A, and table S1). Although

the total rate is far lower, Poly PCs are relatively more prevalent in posterior lobules of mice as well (21.2 versus 10.3%; Fig. 1, F and G, fig. S2A, and table S2).

The broad morphological distributions were consistent across nonpathological human and mouse individuals (fig. S2, B and C, and tables S1 and S2) and did not depend on zonal patl Checing by zebrin II expression (15) (fig. S3). Physical constraints, however, might play a role in the spatial distribution of PC dendrite morphologies by foliar subregion (7). Indeed, the multiple dendrites of Split and Poly PCs predominantly ramified in a horizontal orientation (defined by <30° angle deviation from the PC layer, fig. S4, A and B; see materials and methods) in the sulcus of human folia (80%) while this occurred much less frequently in the bank and gyrus (23 and 25%, respectively; fig. S4D). This effect was not present in mice (fig. S4, C and D). In human PCs—where dendritic size expands strongly (Fig. 1, A and D)—the horizontal orientation follows the inward curvature of the sulcus, possibly indicating a developmental response to physical constraints on growth. Because the physiological implications cannot be readily studied in humans, we turn to the corresponding mouse cells for further characterization.

Multiple CFs may innervate separate primary dendrites

CF activity causes complex spike firing in PCs (16, 17), which is reciprocally related to simple spike firing (17, 18) and exerts powerful control over dendritic integration and PF plasticity (19-26). Though many studies cite the critical importance of one-to-one CF to PC connectivity in cerebellar function, as well as abnormal connectivity in dysfunction, some work has shown CF multi-innervation in ~15% of PCs in adult rodents (27-29).

To test whether multiple CF innervation can be found in mature PCs, we combined a sparse dextran tracer (DA-594) labeling of inferior olivary (IO) neurons (Fig. 2A) with immunolabeling of CF terminal boutons (VGluT2) and PCs (calbindin). Because all CF terminals are marked by VGluT2, but only some will express DA-594, this method allows for the identification of multiple CF inputs from distinct IO neurons onto single PCs (9, 30). Figure 2B shows a Poly PC (P87) that was indeed innervated by two CFs on its separate primary dendrites.

Quantification of CF multi-innervation in mature PCs

We obtained a quantitative measure of CF multi-innervation across the PC population by using whole-cell patch-clamp recordings in murine cerebellar slices (Fig. 2C). We adjusted current intensity and stimulus electrode position in the granule cell layer—subadjacent to each patched PC—to identify any ascending CF inputs and their stimulus thresholds. Mono-innervated PCs had a single, discrete excitatory post-synaptic current (EPSC) amplitude whereas multi-innervated PCs exhibited two or more discrete EPSC amplitudes selectively evoked by distinct stimulus intensities (Fig. 2C, bottom, and fig. S5, A and B). About 15% of all PCs in mature animals (P20-66) received multiple CFs (Fig. 2D, left). CF competition for survival is complete by P20 (8, 9, 28, 31). In keeping with this, we did not find an effect of age on the rate of multi-innervation (fig. S6L).

Combining this technique with fluorescent dye loading and confocal imaging revealed that multi-innervation was largely restricted to PCs with multi-branched structures (23/24 PCs) and occurred in ~25% of cells in this group (1/64 Normative, 15/61 Split, and 8/34 Poly PCs; Fig. 2D). The summed CF EPSC of multi-innervated PCs was larger, on average, than the amplitude of individual CF inputs to mono-innervated PCs (Fig. 2E). The amplitude of the smaller CF (at −30 to −10 mV holding potential) was typically >200 pA (Fig. 2E). This indicates that, under physiological membrane potentials, even the weakest of multiple CFs will likely deliver sufficient current to the soma to influence output (32). The amplitude of weaker CFs increased with age (fig. S5M), which may denote a delayed or elongated maturation period of these inputs relative to the completed development of single CF inputs or the more dominant of multiple CFs (fig. S5N). The relative EPSC amplitude ratio between dominant and smaller CFs varied widely, but smaller CFs most often had >25% the relative amplitude of the dominant CF (fig. S5O). This ratio differed across foliar sub-areas (fig. S5P) and correlated with the angle between Poly PC trunks (fig. S5Q), further emphasizing the relationship between morphology and CF input properties.

The prevalence of multi-innervation was correlated with proximity of bifurcation and angle of separation between emerging trunks in Split and Poly PCs, respectively (Fig. 2, F and H, and fig. S5, D and F). Multi-CF PCs also had wider dendritic arbors in the parasagittal plane (Fig. 2G and fig. S5G), but did not differ in the angle of bifurcation (fig. S2E) or soma size (fig. S5H).

CF multi-innervation was present across cerebellar regions and foliar sub-areas (fig. S6, A to I). Posterior lobules had a higher frequency of multi-innervation (fig. S6I), possibly due to increased prevalence of Poly PCs (fig. S6, H and J), matching our finding in immunolabeled tissue (Fig. 1F and fig. S2A). We did not observe a preferential rate of multi-innervation within the sulcus as a general pattern [but see (29) for more detailed analysis within vermis].

CF multi-innervation produces heterogeneous Ca^{2+} signals across dendrites in vivo

Do multiple converging CFs provide functionally distinct inputs to a single PC? How would this affect dendritic signaling in vivo? To answer these questions, we examined whether CF multi-innervation produces heterogeneous Ca^{2+} signals across separate dendritic branches. CF input triggers massive Ca^{2+} entry into PC dendrites through voltage-gated Ca^{2+} channels (33), NMDA receptors (34), and release from internal stores (35), which can be locally modulated by ion conductance plasticity (33, 36) and interneuron inhibition (37, 38). These mechanisms contribute to the calcium events that we monitor here in vivo and to their modulation (39-41).

We obtained a sparse PC expression of the Ca^{2+} indicator GCaMP6f and used two-photon imaging of mice in a state of quiet wakefulness (awake; no detected motion) to record non-evoked “spontaneous” Ca^{2+} signals from primary dendrite compartments in small populations of <10 cells (Fig. 3, A and B; see materials and methods). Volumetric scans visualized cellular morphology and permitted manual tracing of compartment ROIs (Fig. 3, B and D, and Figs. 4A and 5A) so fluorescence signals were extracted and deconvolved

separately to contrast event amplitude and frequency across branches (Fig. 3, C and E). In this configuration, non-evoked Ca^{2+} signals beyond the micro-compartment scale are almost entirely CF-dependent (42, 43) and Ca^{2+} event amplitude reflects the number of spikes in the presynaptic CF burst (44). This is confirmed by our observed ~1.2 Hz spontaneous Ca^{2+} event frequency (fig. S7D) that matches an expected CF input frequency moderately greater than 1 Hz (17).

We first identified local Ca^{2+} peaks detected in only one branch of each cell (Fig. 3, C, F, and G and movie S1), which were moderately smaller than globally expressed events on average (Fig. 3F). We also compared the inter-event cross-correlation of Ca^{2+} events across branches, for which the fit and significance of a linear regression describes the interbranch covariation (Fig. 3, H and I).

Most PCs had homogenous Ca^{2+} signals with linear inter-event covariance relationships across branches (Adj $R^2 > 0.1$) and low numbers of local events (Fig. 3, G and H). However, some PCs exhibited Ca^{2+} signal heterogeneity characterized by a linear regression of inter-event covariation with low Adj $R^2 < 0.1$ that was not significant (0, 15, and 38% of Normative, Split, and Poly PCs, respectively; Fig. 3, H and I) or a higher ratio of local events (17.4, 36.6, and 51%; Fig. 3G). High variability of inter-event amplitude scale between branches, another measure of heterogeneity, correlated with the bifurcation distance and total parasagittal dendritic width (Fig. 3, J and K, and fig. S7C). This further links heterogeneity to underlying morphological contours defined by primary dendrite geometry. Confirming that local events are the product of additional CF input, PCs with high local event rates had higher mean (fig. S7, G, H, and P) and maximum total event rates (fig. S7, L and M), producing a larger dynamic range (fig. S7, N and O). Our observations link the occurrence of local CF events to underlying morphological contours defined by primary dendrite geometry, although other factors, such as inhibition by molecular layer interneurons (MLIs), are likely to contribute as well (37, 42).

CFs convey distinct whisker receptive fields to separate primary dendrites

To identify CF receptive fields (RFs) and their localization on PC dendrites, we took advantage of the discrete organization of whiskers as a sensory input array (45, 46). We anaesthetized animals to stimulate untrimmed individual whiskers at 2 Hz for 50 s periods while recording Ca^{2+} activity of PCs in medial Crus I (Fig. 4A and fig. S8A; see materials and methods). Most PCs had only global events identically represented across primary dendrites (figs. S8, A2, and A3). However, some PCs had high numbers of local events in response windows during the stimulus period (Fig. 4, B and C, and fig. S8 A4) that varied in magnitude between distinct whisker stimuli (Fig. 4D), indicating RF selectivity.

Anaesthetized activity is sparsened, so responses were determined using the z-scored response probability during the experimentally bootstrapped high-frequency stimulus (fig. S8, B to D). Comparing the z-scored response probability of each dendrite, we observed a “lateralized” response in some PCs, in which local events of one branch constituted a whisker response not observed in the other branch (Fig. 4, E and F). Nearly all lateralized responses arose in Split and Poly PCs (48/52 cells, 92%; Fig. 4F) and in PCs with

more spontaneous signal heterogeneity, which map to Split and Poly PCs as in previous experiments (fig. S8F). Furthermore, PCs with lateralized responses had more proximal dendrite bifurcations than PCs with only global responses (18.73 μm versus 28.24 μm; Fig. 4G). Notably, PCs with higher rates of branch-specific spontaneous events also exhibited responses to more whiskers, denoting an integration of more whiskers into their RFs (Fig. 4H). This supports the hypothesis that heterogeneous signals represent distinct, converging RFs such that heterogeneous PCs are sampling more upstream RFs carried by functionally independent CF inputs.

CF-induced branch-specific representations of stimulus modality in awake mice

Although anesthesia provided excellent control and precision for single whisker stimulation, even subanesthetic ketamine alters network activity (47). To confirm that PC primary dendrites can differentially represent CF RFs in a more naturalistic state, we exposed awake animals to uni- and multisensory stimuli (Fig. 5A). As a major hub for sensory integration during associative learning, PC dendrites are an important model for how converging input profiles are represented across dendrites. The amplitude and duration of CF-induced dendritic Ca^{2+} spikes depend on stimulus strength (43, 48), which is reflected in CF burst behavior (44) and also on synaptic connectivity and weight of the CF input itself (49).

We stimulated awake animals with light (488 nm, ipsilateral), sound (12 kHz tone, bilateral), and peri-oral air puff (10 psi, ipsilateral) stimuli either alone or in multimodal combinations while recording response properties in PC primary dendrites. Sensory-evoked events, more than spontaneous, typically produced a global dendritic signal with consistent intertrial amplitude ratio between branches (Fig. 5B1). However, we also observed complex sensory-evoked bursts of CF input with heterogeneous amplitudes between branches (Fig. 5, B2 and B3) and either branch-specific responses alone (Fig. 5B4) or combined with a global response (Fig. 5B2). Whereas PCs with multiple primary dendrites [Split and Poly (S/P)] had similar total response probabilities as Normative PCs (fig. S9C), a larger share of responses were branch-specific in S/P PCs across stimulus modalities (Fig. 5, C and D, and fig. S9, A and B). To assess the relationship between uni- and multimodal stimuli, we identified themaximum branch-specific responses to stimuli of each category (fig. S9D), obtained the difference between uni- and multisensory maxima, and found an enhanced rate of local responses in S/P but not Normative PCs (fig. S9F). This revealed that multisensory stimuli could enhance the differential representation of CF RFs across primary dendrites in utatively multi-innervated PCs while failing to influence mono-innervated Normative PCs.

While the previous analyses were blind to branch identity, we next asked how much the differential representation of each stimulus could favor one branch over the other (fig. S9E). We generated a Δ Branch Response (ΔBR) index for each stimulus modality by calculating the difference in branch-specific, local responses as a fraction of total responses (Fig. 5E, top). Absolute ΔBR indicates the reliability of local responses on either branch whereas the sign of the ΔBR indicates which branch over-represented themodality. This allowed us to generate a profile of branch-specific representation across all stimulus modalities, which

could be quantified by the ΔBR mean and range for each cell (Fig. 5E, bottom). In this way, PCs could be distinguished as having one of three classes of multisensory response profiles: global, with identical representation across branches in all cases; unilateral, with one branch exhibiting a larger RF representation than the other; and bilateral, with both branches capable of differentially representing unique stimulus modalities.

On average, S/P cells had a wider range, denoting branch-specific (e.g., unilateral or bilateral) representations that were more distinct across modalities (Fig. 5F and fig. S9, G to I). Cells for which only one branch exhibits local responses—that is, unilateral—would have both a large ΔBR range but also a ΔBR mean that deviates from zero to favor that branch. To better characterize whether some PCs had bilateral representation profiles, we calculated the bilaterality of the RF profile by subtracting the ΔBR mean from the range. The local responses of S/P cells, more than Normative, produced RF profiles wherein a larger percentage of local signaling produced bilateral representations across sensory modalities (Fig. 5H and fig. S9, G, H, and K). Collectively, this shows that PCs with multiple primary dendrites can differentially represent RFs of distinct CF inputs across their separate dendrites in awake, mature mice (for a summary of heterogeneous signaling observed in our two-photon recordings across the three dendrite morphologies in mouse PCs, see fig. S10).

Discussion

We found that noncanonical CF multi-innervation of PCs does occur in the mature murine cerebellum and is dependent on primary dendrite morphology. Nearly all observed multi-innervation occurred in neurons with multiple primary dendrites. Based on a quantitative categorization of >6000 PCs from three human brains, we report that this type of PC dendritic structure is predominant in the human cerebellum. By contrast, we detected that only a minority of murine PCs fall into the Split or Poly category. Within these morphological groups, about 25% of PCs were innervated by two or more CFs in the mouse.

Our two-photon recordings suggest that most multi-innervated PCs have the capacity for branch-specific CF signaling and have distinct CF RFs. Our data do not allow us to conclude that the same results would be found in human PCs if such recordings were possible. However, they do describe a new motif in PC dendritic compartmentalization: separate dendritic subfields with their own assigned CF inputs may emerge when early branching forms a multibranched architecture. Variable CF burst frequency and modulation of CF input amplitude by MLIs may further contribute to compartmentalization (37, 42).

CFs provide instructive signals in cerebellar function and plasticity (17) by encoding signals related to error (19, 50), sensory omission (51), as well as reward or reward-prediction (52, 53). Our findings constitute a substantial shift from the currently held belief that one CF innervates each PC. Instead, our observations suggest that one CF innervates each primary dendrite.

The consequences for dendritic integration and, ultimately, the activation of target cells in the cerebellar nuclei (54) are potentially multifold. Here, we discuss those that immediately

result from geometric considerations. Multibranched structure often increases dendritic width in the sagittal plane (Fig. 3K), in some cases even opening a cleft between compartments (see Fig. 1, A and D, Figs. 3B and 4E, fig. S1, B and C, and fig. S4B). This configuration inevitably leads to a wider physical gap between innervating PF bundles and thus to a potential functional separation of the contextual information they provide (55, 56). It is therefore conceivable that PCs drive spike output from a multitude of contextual input combinations that expand with increased dendrite size and complexity. Multiple CF innervation that, as we describe here, occurs at an elevated rate in multibranched PCs may serve several critical purposes. First, it may enhance PC function as a supervised associative learning perceptron that optimizes synaptic weights (57) by providing RF-matched CF inputs—and thus relevant errors and instructive signals—to the different PF inputs that convey specific contextual information (fig. S11A). In this way, the perceptron orchestrates synaptic weight optimization based on compartmentalized, rather than all-dendritic, instructive signals. Thus, in receiving multiple CF inputs, some PCs are permitted to fully capitalize on diverse context representations surveyed by their multibranched architecture. Second, multiple CF innervation may enable more complex PC computations, such as multiplexing and conveying input from a wider array of sensory modalities (fig. S11B). In this scenario, individual multibranched PCs may pair different contexts presented by their PF inputs with instructive information collected from a multimodal environment.

In both the human and mouse cerebellum, multibranched PCs are more prevalent in the posterior cerebellar hemisphere, a region linked to cognitive and affective roles (58-60). Whether or not the multibranched architecture enables such complex functions through the gained computational power that is postulated here needs to be investigated in future studies.

On the other hand, excessive CF-PC strength resulting from disrupted synaptic pruning and ectopic innervation of distal PC dendrites is linked to pathological dysfunction in autism model mice (27, 49) mouse and human essential tremor (61). The preferential targeting of distinct primary dendrites by multiple CFs (Fig. 2B) may bring computational advantages while avoiding disruptive enhancement of CF inputs to individual dendritic compartments.

Supplementary Material

Refer to Web version on PubMed Central for supplementary material.

ACKNOWLEDGMENTS

For valuable advice and technical support, we thank Hansel lab members T. F. Lin, A. Silbaugh, and T. Pham. We thank R. A. Eatock and P. Mason (UChicago Neurobiology) for insightful discussions. For crucial feedback on the manuscript, we thank W. Wei and M. Sheffield (UChicago Neurobiology) as well as S. S. Wang (Princeton). M. Sheffield and S. S. Wang also provided preliminary viral tools. Human tissue made available by the Anatomical Gift Association of Illinois.

Funding:

This work was supported by the following: National Institutes of Health (NINDS) grant R21NS124217 (to C.H.); National Institutes of Health (NINDS) grant F31NS129256 (to S.E.B.); and The University of Chicago Pritzker Fellowship (to S.E.B.)

REFERENCES AND NOTES

1. Apps R, Hawkes R, Nat. Rev. Neurosci 10, 670–681 (2009). [PubMed: 19693030]
2. Nedelescu H, Abdelhack M, Pritchard AT, J. Neurosci. Res 96, 1476–1489 (2018). [PubMed: 29319237]
3. Golgi C, Sulla fina anatomia del cervelletto umano (Archivio Italiano per le Malattie Nervose, 1874), vol. 2.
4. Ramón y Cajal S, Histologie du système nerveux de l'homme and des vértebrés (Paris: Maloine, 1909).
5. Kato T, Hirano A, Llena JF, Acta Neuropathol. 68, 145–148 (1985). [PubMed: 4072621]
6. Louis ED et al., Brain 137, 3142–3148 (2014). [PubMed: 25367027]
7. Eccles JC, Ito M, Szentagothai J, The Cerebellum as a Neuronal Machine (Springer, 1967).
8. Hashimoto K, Kano M, Neuron 38, 785–796 (2003). [PubMed: 12797962]
9. Hashimoto K, Ichikawa R, Kitamura K, Watanabe M, Kano M, Neuron 63, 106–118 (2009). [PubMed: 19607796]
10. Wilson AM et al., Cell Rep. 29, 2849–2861.e6 (2019). [PubMed: 31775050]
11. Hansel C, Linden DJ, Neuron 26, 473–482 (2000). [PubMed: 10839365]
12. Bosman LWJ, Takechi H, Hartmann J, Eilers J, Konnerth A, J. Neurosci 28, 798–807 (2008). [PubMed: 18216188]
13. Ohtsuki G, Hirano T, Eur. J. Neurosci 28, 2393–2400 (2008). [PubMed: 19032589]
14. Piochon C, Kano M, Hansel C, Nat. Neurosci 19, 1299–1310 (2016). [PubMed: 27669991]
15. Cerminara NL, Lang EJ, Sillitoe RV, Apps R, Nat. Rev. Neurosci. 16, 79–93 (2015). [PubMed: 25601779]
16. Eccles JC, Llinás R, Sasaki K, J. Physiol 182, 268–296 (1966). [PubMed: 5944665]
17. Simpson JI, Wylie D, De Zeeuw CI, Behav. Brain Sci 19, 384–398 (1996).
18. Badura A et al., Neuron 78, 700–713 (2013). [PubMed: 23643935]
19. Ito M, Sakurai M, Tongroach P, J. Physiol 324, 113–134 (1982). [PubMed: 7097592]
20. Wang SS-H, Denk W, Häusser M, Nat. Neurosci 3, 1266–1273 (2000). [PubMed: 11100147]
21. Lev-Ram V, Wong ST, Storm DR, Tsien RY, Proc. Natl. Acad. Sci. U.S.A 99, 8389–8393 (2002). [PubMed: 12048250]
22. Medina JF, Nores WL, Mauk MD, Nature 416, 330–333 (2002). [PubMed: 11907580]
23. Coesmans M, Weber JT, De Zeeuw CI, Hansel C, Neuron 44, 691–700 (2004). [PubMed: 15541316]
24. Piochon C et al., Proc. Natl. Acad. Sci. U.S.A 113,13221–13226 (2016). [PubMed: 27799554]
25. Streng ML, Popa LS, Ebner TJ, J. Neurosci 37, 1997–2009 (2017). [PubMed: 28077726]
26. Titley HK, Kislin M, Simmons DH, Wang SS-H, Hansel C, J. Physiol 597, 4387–4406 (2019). [PubMed: 31297821]
27. Piochon C et al., Nat. Commun 5, 5586 (2014). [PubMed: 25418414]
28. Kano M et al., Neuron 18, 71–79 (1997). [PubMed: 9010206]
29. Nishiyama H, Linden DJ, J. Neurosci 24, 3926–3932 (2004). [PubMed: 15102908]
30. Miyazaki T, Watanabe M, Anat. Sci. Int 86, 10–18 (2011). [PubMed: 21153457]
31. Kano M, Watanabe T, Uesaka N, Watanabe M, Cerebellum 17, 722–734 (2018). [PubMed: 30009357]
32. Llano I, Marty A, Armstrong CM, Konnerth A, J. Physiol 434, 183–213 (1991). [PubMed: 1673717]
33. Schmolesky MT, Weber JT, De Zeeuw CI, Hansel C, Ann. N. Y. Acad. Sci 978, 359–390 (2002). [PubMed: 12582067]
34. Piochon C, Levenes C, Ohtsuki G, Hansel C, J. Neurosci 30, 15330–15335 (2010). [PubMed: 21068337]
35. Takechi H, Eilers J, Konnerth A, Nature 396, 757–760 (1998). [PubMed: 9874373]
36. Ohtsuki G, Piochon C, Adelman JP, Hansel C, Neuron 75, 108–120 (2012). [PubMed: 22794265]

37. Callaway JC, Lasser-Ross N, Ross WN, J. Neurosci 15, 2777–2787 (1995). [PubMed: 7722628]
38. Rowan MJM et al., Neuron 99, 999–1015.e6 (2018). [PubMed: 30122378]
39. Kitamura K, Häusser M, J. Neurosci 31, 10847–10858 (2011). [PubMed: 21795537]
40. Zang Y, Dieudonné S, De Schutter E, Cell Rep. 24,1536–1549 (2018). [PubMed: 30089264]
41. Roome CJ, Kuhn B, Nat. Commun 9, 3388 (2018). [PubMed: 30139936]
42. Najafi F, Giovannucci A, Wang SS-H, Medina JF, Cell Rep. 6, 792–798 (2014). [PubMed: 24582958]
43. Gaffield MA, Bonnan A, Christie JM, Neuron 102, 762–769. e4 (2019). [PubMed: 30928170]
44. Roh S-E et al., eLife 9, e61593 (2020). [PubMed: 32985976]
45. Bosman LWJ et al., J. Physiol 588, 3757–3783 (2010). [PubMed: 20724365]
46. Ju C et al., J. Physiol 597, 2483–2514 (2019). [PubMed: 30908629]
47. Cichon J et al., Nat. Neurosci 26, 39–52 (2022). [PubMed: 36424433]
48. Najafi F, Giovannucci A, Wang SS-H, Medina JF, eLife 3, e03663 (2014). [PubMed: 25205669]
49. Simmons DH et al., Biol. Psychiatry Glob. Open Sci 2, 450–459 (2021). [PubMed: 36324646]
50. Yang Y, Lisberger SG, Nature 510, 529–532 (2014). [PubMed: 24814344]
51. Ohmae S, Medina JF, Nat. Neurosci 18, 1798–1803 (2015). [PubMed: 26551541]
52. Heffley W, Hull C, eLife 8, e46764 (2019). [PubMed: 31509108]
53. Kostadinov D, Beau M, Blanco-Pozo M, Häusser M, Nat. Neurosci 22, 950–962 (2019). [PubMed: 31036947]
54. Person AL, Raman IM, Nature 481, 502–505 (2011). [PubMed: 22198670]
55. Wilms CD, Häusser M, Nat. Commun 6, 6464 (2015). [PubMed: 25751648]
56. Nguyen TM et al., Nature 613, 543–549 (2023). [PubMed: 36418404]
57. Brunel N, Hakim V, Isope P, Nadal J-P, Barbour B, Neuron 43, 745–757 (2004). [PubMed: 15339654]
58. Stoodley CJ, Schmahmann JD, Cortex 46, 831–844 (2010). [PubMed: 20152963]
59. Badura A et al., eLife 7, e36401 (2018). [PubMed: 30226467]
60. LeBel A, Jain S, Huth AG, J. Neurosci 41, 10341–10355 (2021). [PubMed: 34732520]
61. Pan M-K et al., Sci. Transl. Med 12, eaay1769 (2020). [PubMed: 31941824]
62. Busch S, Climbing fiber multi-innervation of mouse Purkinje dendrites with arborization common to human, Dryad (2023); 10.5061/dryad.kh18932c1.

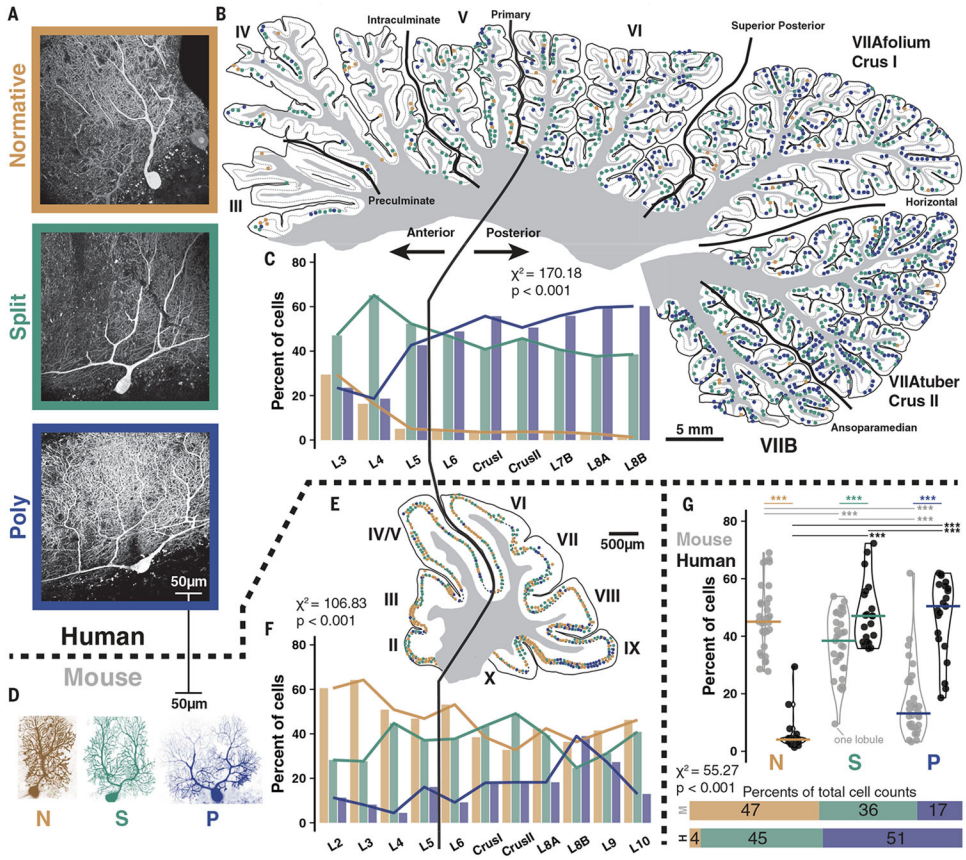

Fig. 1. Comparative morphology and regional variability in human and mouse cerebellar PCs.

(**A**) Immunolabeling of PCs in humans reveals a range of dendritic morphologies, categorized by primary dendrite geometry as Normative, Split, or Poly. (**B**) Human mid-hemisphere reconstruction demonstrating the spatial distributions of each morphological type. As a result of variable preservation of tissue some anterior lobules and intervening posterior sublobules had a lower density of labeled PCs. (**C**) Morphology demographics across lobules (n = 3 individuals >86 years old, 6640 cells; see table S1). (**D**) PCs filled with dye during a patch experiment in mice to scale with human cells also exhibit Normative, Split, and Poly morphology. (**E** and **F**) as in (B and C), but in mice (n = 3 mice >P50, 1350 cells; see table S2). (**G**) Morphological category distribution counted by lobule (top) in human (n = 20, 21, and 21 lobules) and mouse (n = 30, 30, 29) reveals a consistent increase in the number of Split and Poly PCs in human matching the rates of the whole cell population (bottom). Average lines depict median lobule value. *P < 0.05, **P < 0.01, ***P < 0.001.

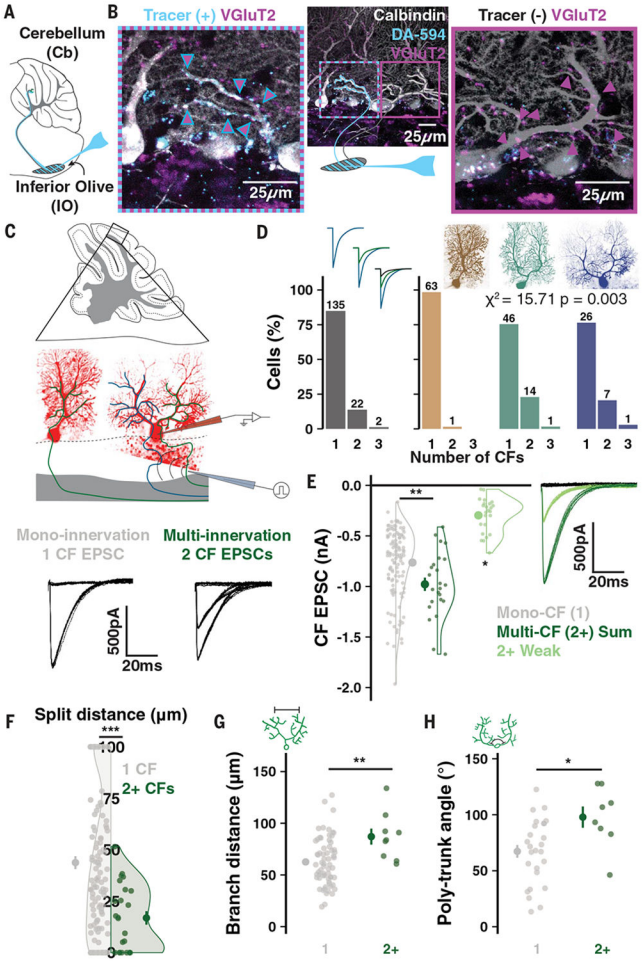

Fig. 2. CF multi-innervation of mature multibranched PCs.

(**A**) Schematic of tracer (DA-594) injection. (**B**) A Poly PC after immunolabeling for PCs (calbindin) and CF terminals (VGluT2). The tracer label distinguishes CFs with distinct olivary origin on the left and right trunks. (**C**) Scheme of whole-cell patch-clamp in cerebellar slices and CF EPSCs recorded from either a mono- or multi-innervated PC. (**D**) Number of mono- versus multi-innervated PCs as a combined population (left). Categorizing by morphology reveals that effectively all multi-innervation occurs in multibranched PCs (n = 50 animals, 159 cells). (**E**) Summed multi-CF EPSCs are larger than mono-CF EPSCs (n = 135 and 24 cells). The weaker of multiple CFs typically provides >200 pA signals. Holding potential: −10 to −30mV (n = 24 cells). (**F**) Multi-innervated PCs have earlier dendrite bifurcations (n = 135 and 24 cells). (**G**) Among PCs with a bifurcated primary dendrite, multi-innervated cells have a wider distance between compartments (n = 85 and 9 cells). (**H**) Multi-innervated Poly PCs have a wider angle between emerging trunks (n = 26 and 8 cells). Summary points indicate mean ± SEM. *P < 0.05, **P < 0.01, ***P < 0.001.

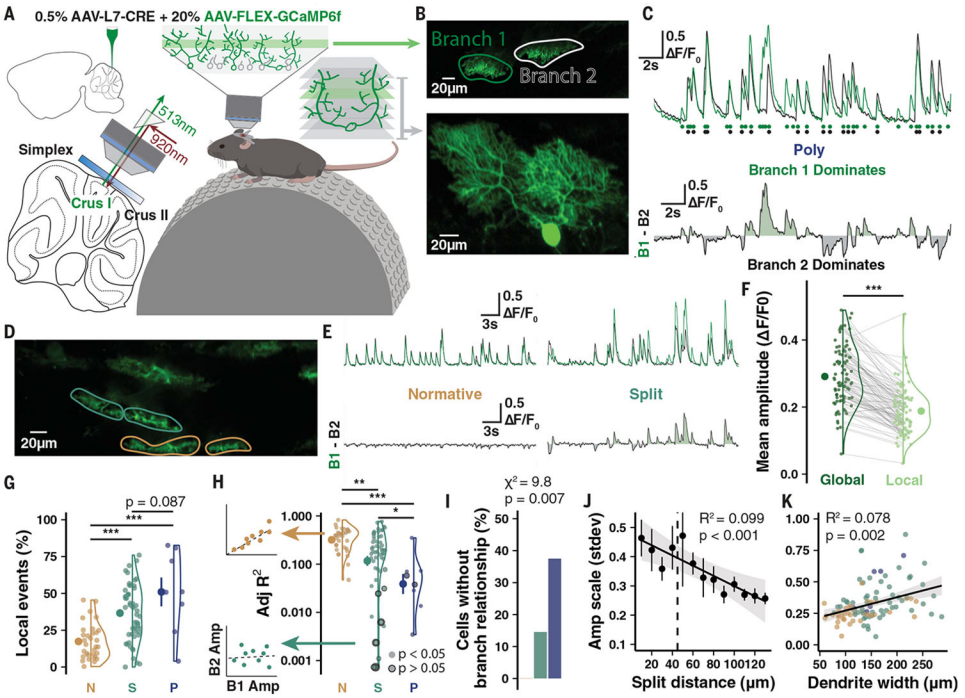

Fig. 3. Two-photon imaging in vivo reveals Ca^{2+} signal heterogeneity across PC dendrites.

(**A**) Schematic of experimental preparation. (**B**) Example imaging plane and three-dimensional reconstruction of a Poly PC. (**C**) Spontaneous signal and deconvolved events (circles) by branch with difference trace below demonstrates heterogeneous global event amplitude scale and branch-specific events. (**D** and **E**) Another recording from a Normative and Split PC highlights homogeneous versus heterogeneous signaling. (**F**) Local events are moderately smaller than global events (n = 15 animals, 95 cells). (**G**) Branch-specific local events as a percentage of total events in each cell by morphology (n = 15 animals; n = 32, 55, and 8 cells). (**H**) Linear regressions on branch cross-correlation quantifies branch similarity (left). Model fit R^2 values (right) reveals that cells with low branch signal similarity are predominantly Split and Poly PCs (n = 32, 55, and 8 cells). Bordered points indicate nonsignificant covariance. (**I**) Cells lacking detectable relationship using regression on interbranch amplitudes are all Split or Poly PCs. (**J** and **K**) Interbranch amplitude variation by Split distance (n = 105 cells) and total parasagittal width of the dendrites (n = 109 cells). Summary points indicate mean ± SEM. *P < 0.05, **P < 0.01, ***P < 0.001.

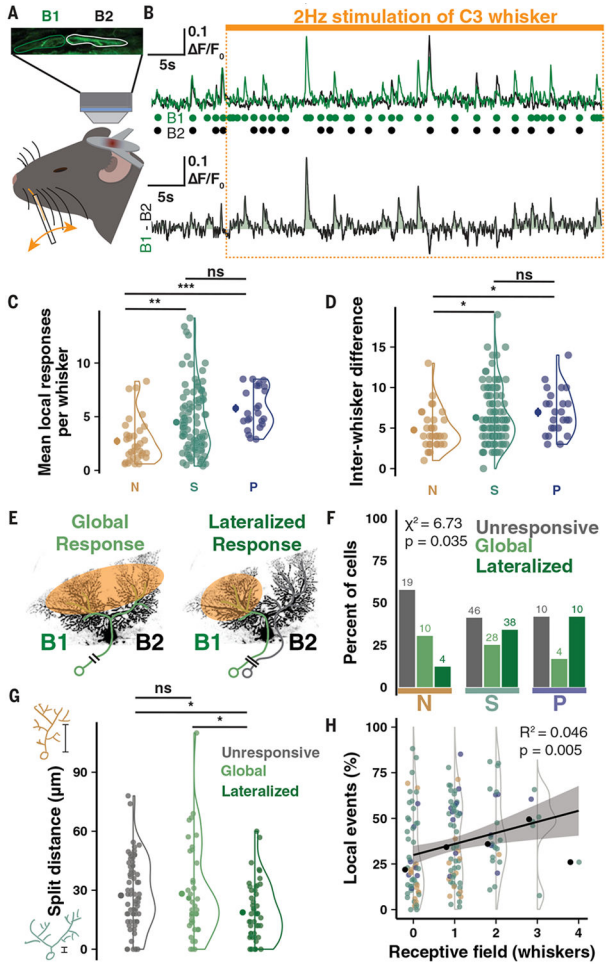

Fig. 4. Branch-specific whisker receptive fields produced by CF multi-innervation of multibranched PCs.

(**A**) Schematic of the imaging configuration and whisker stimulation under anesthesia. (**B**) Sample traces and deconvolved events by branch during 50 s whisker stimulation. Each whisker is tested twice; data from both periods are combined. Responsiveness of one branch and not the other drives an enhanced local event rate in B1 during the stimulus period. (**C**) Mean number of local branch events in response windows during stimulus periods of each tested whisker (n = 13 animals P95-120, n = 33, 112, and 24 cells). (**D**) Difference in local event number between whiskers eliciting maximum and minimum local responses (n = 33, 112, and 24 cells). (**E**) Schematic of global versus lateralized responses. (**F**) Percentage of PCs by dendritic response profile and morphological category. Fewer Normative PCs have lateralized responses than multibranched PCs (n = 169 cells). (**G**) Cells with lateralized responses have shorter Split distances (n = 75, 42, and 52 cells). (**H**) Cells with more spontaneous local events respond to a higher number of whiskers (n = 151 cells). Summary points indicate mean ± SEM. *P < 0.05, **P < 0.01, ***P < 0.001.

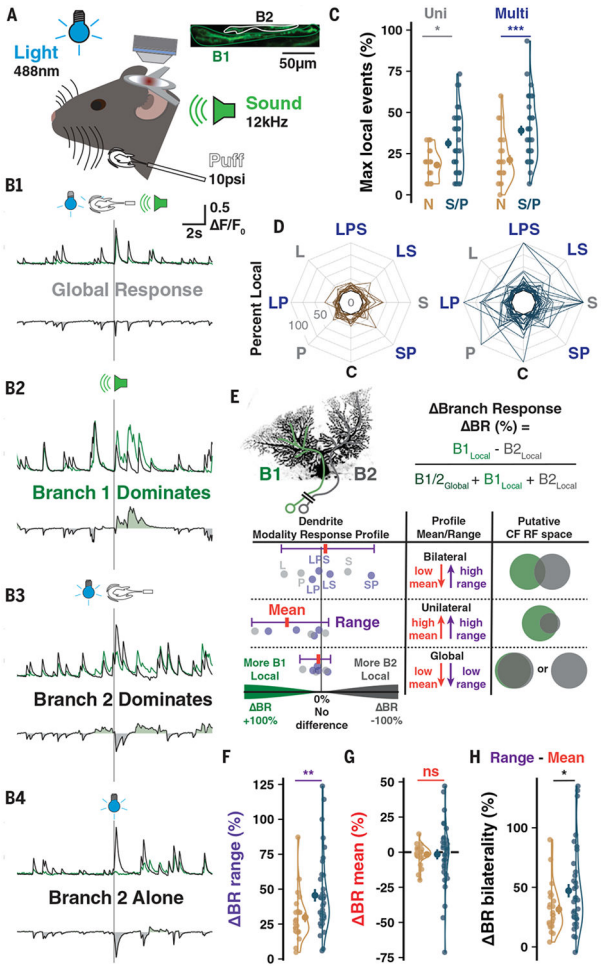

Fig. 5. Branch-specific multisensory receptive fields.

(**A**) Scheme of imaging and sensory stimulation of awake animals. (**B**) Sample traces showing combinations of inter-branch responses to different stimulus modalities. (**C**) The maximum number of local events observed for a stimulus of any category in Normative vs Split and Poly (S/P) PCs (here and below: $n = 12$ animals, $n = 24$ and 38 cells). (**D**) The percentage of responses having a local component, regardless of branch identity, across control (C), uni-, or multisensory trials. Lines connect values for each PC. (**E**) Calculation of ΔBR (top) between the stimulus types most favoring opposite branches. ΔBR values of each modality are calculated for each cell (bottom, schematic points) to map the ΔBR profile across stimuli and identify the mean and range. (**F**) The range is more pronounced in S/P cells ($n = 24, 38$). (**G**) No group difference in ΔBR mean ($n = 24, 38$). (**H**) Response profile bilaterality is the subtraction of DBR mean from the range. S/P PCs exhibit more bilaterality due to high ranges and low means ($n = 24, 38$). Summary points indicate mean ± SEM. $*P < 0.05$, $**P < 0.01$, $***P < 0.001$.